Molecular structure, glass transition temperature variation, agglomeration theory, and network connectivity of binary P-Se glasses

D. G. Georgiev, M. Mitkova, and P. Boolchand
Department of Electrical and Computer Engineering and Computer Science, University of Cincinnati, Cincinnati, Ohio 45221-0030

G. Brunklaus and H. Eckert
Institut für Physikalische Chemie, Westfaelische Wilhelms Universitaet Muenster, D-48149 Munster, Germany

M. Micoulaut
Laboratoire de Physique Théorique des Liquides, Université Pierre et Marie Curie, Tour 16, 4 Place Jussieu, 75252 Paris Cedex 05, France

(Received 22 February 2000; revised manuscript received 23 May 2001; published 29 August 2001)

Raman scattering and ^{31}P NMR results show that the backbone of binary P_xSe_{1-x} glasses is composed of Se_n-chain fragments, pyramidal $P(Se_{1/2})_3$ units, quasitetrahedral $Se{=}P(Se_{1/2})_3$ units, and ethylenelike $P_2(Se_{1/2})_4$ units at low P content ($x<0.47$). Concentrations of the various building blocks independently established from each spectroscopic probe are found to be correlated. Theoretical predictions for the glass transition variation $T_g(x)$ from agglomeration theory are compared to the observed $T_g(x)$ trends established from temperature-modulated differential scanning calorimetry. The comparison shows that a stochastic network description is an appropriate one of glasses at low x ($x<0.12$). At medium x ($0.12<x<0.47$), substantial medium-range structure evolves in the form of polymeric ethylenelike units that comprise elements of the barely rigid backbone. At higher x ($x>0.47$), a rapid phase separation of monomeric P_4Se_3 units from the backbone takes place, leading to a molecular glass with a rather low T_g at $x>0.50$.

DOI: 10.1103/PhysRevB.64.134204 PACS number(s): 61.43.Fs, 63.50.+x, 61.18.Fs, 61.20.−p

I. INTRODUCTION

Bulk glass formation in the P_xSe_{1-x} binary occurs over wide compositions[1] $0<x<0.80$, with a narrow window $0.52<x<0.60$ centered at $x=0.57$ corresponding to the P_4Se_3 stoichiometry across which melts display a propensity for crystallization rather than glass formation. Melts in the window usually form molecular solids composed of P_4Se_3 monomers. The monomer consists[2] of a triangular $P_3(Se_{1/2})_3$ prism capped by a pyramidal $P(Se_{1/2})_3$ unit (Fig. 1). As a solid, P_4Se_3 exists in two ordered (α,α') low-T phases and two orientationally disordered (β, γ) phases prior to melting at 244 °C. Transformations[3] between these polymorphs have been established by differential scanning calorimetry (DSC). Raman spectra of the polymorphs have also been studied.[4] Furthermore, crystalline P_4Se_4 phases (α, β) have also been synthesized and characterized by x-ray and Raman scattering.[5,6] The variety of building blocks occurring in the present binary are illustrated in Fig. 1, including the P_4Se_4 monomer structures in the α and β phases. Upon melting β-P_4Se_4, melts possessing a polymeric structure are formed and consist of ethylenelike $P_2(Se_{1/2})_4$ units. Such structures apparently constitute an important part of the backbone of binary P-Se glasses in the $0.20<x<0.50$ range, as will become transparent later.

The molecular structure of the Se-rich ($0<x<0.52$) and P-rich ($0.60<x<0.80$) glasses has been the subject of previous investigations by differential scanning calorimetry,[6] diffraction methods,[7–9] Raman scattering,[10] and ^{31}P and ^{77}Se solid-state NMR.[11,12] ^{31}P NMR chemical shifts of these building blocks have been established.[13] Raman scattering provides a powerful complementary probe to establish details of glass structure. Because of the diversity and complexity of glass structure and Raman lineshapes, particularly at $x<0.50$, deconvolution of Raman line shapes and microscopic identification of vibrational modes have been a challenge.

In this work we have examined Se-rich glasses ($0<x<0.52$) in Raman scattering and ^{31}P NMR measurements. Raman and NMR results on the crystalline reference com-

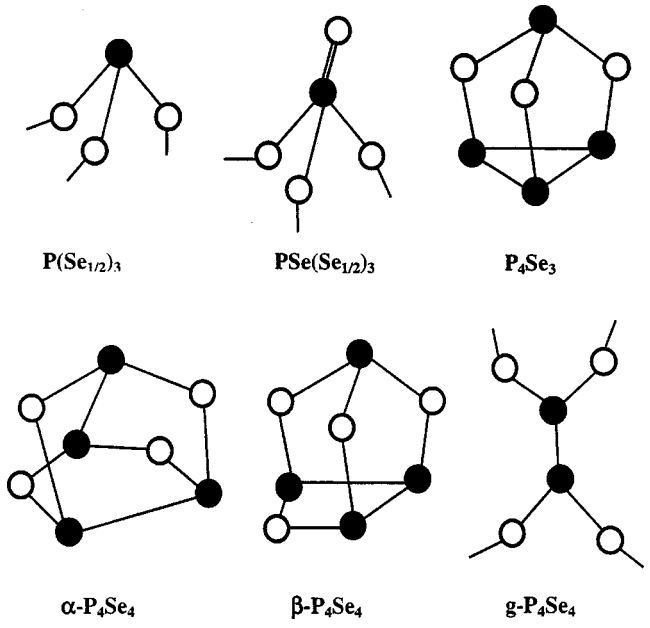

FIG. 1. Local building blocks of the P-Se glass system.

pounds P_4Se_3 and P_4Se_4 have served as an important aid in mode and site assignments, permitting us to decode the structure of these glasses on an atomic level. In addition to pyramidal $P(Se_{1/2})_3$ units, our experiments show that polymeric ethylenelike $P_2(Se_{1/2})_4$ units and quasitetrahedral $Se{=}P(Se_{1/2})_3$ units also occur in the Se-rich glasses ($x < 0.50$). Glass transition temperatures (T_g) are studied[14] by temperature-modulated differential scanning calorimetry (MDSC). The observed $T_g(x)$ variation is analyzed in terms of glass structure results using agglomeration theory.[15] As we will demonstrate, this analysis shows that the $T_g(x)$ variation serves as a good measure of network connectivity, and at low x (<0.12), the agglomeration of the network is stochastic in character.

II. EXPERIMENTAL RESULTS

A. Sample synthesis

P_xSe_{1-x} glasses in the $0<x<0.52$ composition range were synthesized using 99.999% Se and P lumps as starting materials from Cerac Inc. The elements were handled in a glove bag purged with dry-N_2 gas and reacted at 650 °C for at least 72 h in evacuated (2×10^{-7} Torr) quartz ampoules. After equilibrating the samples at 400 °C, the ampoules were water quenched to realize micaceous glass samples with colors ranging from black to reddish brown as the P content increased to $x=0.50$.

Samples of c-P_4Se_3 were prepared by reacting the elements in the desired ratio and slow cooling the melt. Samples of c-P_4Se_4 were synthesized by reacting an intimate finely ground mixture of c-P_4Se_3 and elemental Se in the stoichiometric ratio, and heating at 330 °C for 72 h. Two glass samples were prepared from this material upon heating to its melting temperature ($T_m=340$ °C) for a short time (90 min) and an extended period (3 h), respectively. These samples were examined by Raman scattering and ^{31}P NMR and revealed striking differences in molecular structure as will be discussed later.

B. Thermal characterization

We used a model 2920 temperature-modulated DSC from TA Instruments, Inc. to establish the glass transition temperatures (T_g's) of the P_xSe_{1-x} glasses. A heating rate of 3 °C/min and a modulation rate of 1 °C per 100 s were used for all scans. Scans were made both increasing in T past T_g and decreasing in T from T_g. The inflection point of the *total heat flow* endotherm was taken as $T_g^{\rm app}$, while that of the *reversing heat flow* endotherm was taken as T_g. In general, $T_g>T_g^{\rm app}$ because the presence of a kinetic heat flow, also called the *nonreversing heat flow* ($\Delta H_{\rm nr}$), as a precursor to the actual glass transition.

Figure 2(a) shows a summary of $T_g(x)$ variation in the present glasses. Figure 2(b) compares the present $T_g^{\rm app}(x)$ with the published[16] glass transitions on the present binary glasses from previous work using DSC. In Fig. 2(b), in each instance, one is comparing the glass transition temperature deduced from the *total heat flow*, one using an MDSC, and all others using DSC instruments. The agreement between various results is reasonable. A noteworthy feature of the $T_g(x)$ trend in Fig. 2(a) is its smoothness and almost flat variation with x in the $0.20<x<0.45$ range, followed by a steep increase at $x>0.45$. On the other hand, the $T_g^{\rm app}$ trend provides some evidence of a discontinuity near $x=0.30$, a feature also noted by previous workers.[6] The latter is an artifact resulting from the use of the total heat flow to extract T_g's ($T_g^{\rm app}$). Shifts in $T_g^{\rm app}$ result due to kinetic effects associated with nonreversing heat flow term. Such shifts are nearly eliminated when T_g's are extracted from the reversing heat flow term [Fig. 2(a)].

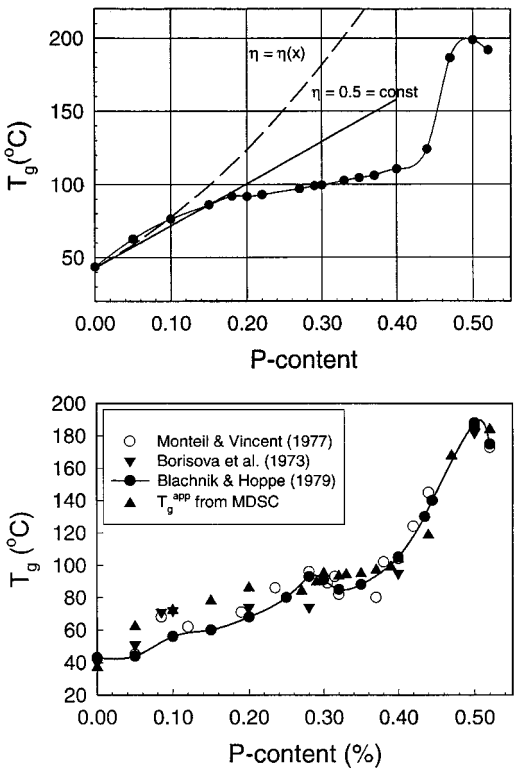

FIG. 2. MDSC measured $T_g(x)$ variation in P_xSe_{1-x} glasses. The smooth line through the data points is a guide to the eye. The dashed line is the $T_g(x)$ prediction of agglomeration theory. (b) $T_g^{\rm app}(x)$ variation deduced from total heat flow in MDSC and DSC measurements. The latter are taken from previous publications as indicated. The threshold behavior near $x=0.24$ in $T_g^{\rm app}$ is an artifact as discussed in text.

C. Raman scattering

Raman-Stokes spectra of freshly fractured surfaces of the glasses were taken at room temperature using an Instruments SA model T64000 Raman facility, equipped with a triple monochromator, liquid-N_2-cooled charge-coupled device (CCD) detector and a microscope. Typically less than 1 mW of 647.1 nm radiation from a Kr^+ ion laser was used to excite the scattering. Sample homogeneity was verified by comparing spectra on a 2-μm spatial resolution using a microscope attachment. We also recorded spectra of the glasses in the fused quartz ampoules used to synthesize them. Spectra of the samples taken in laboratory ambient looked iden-

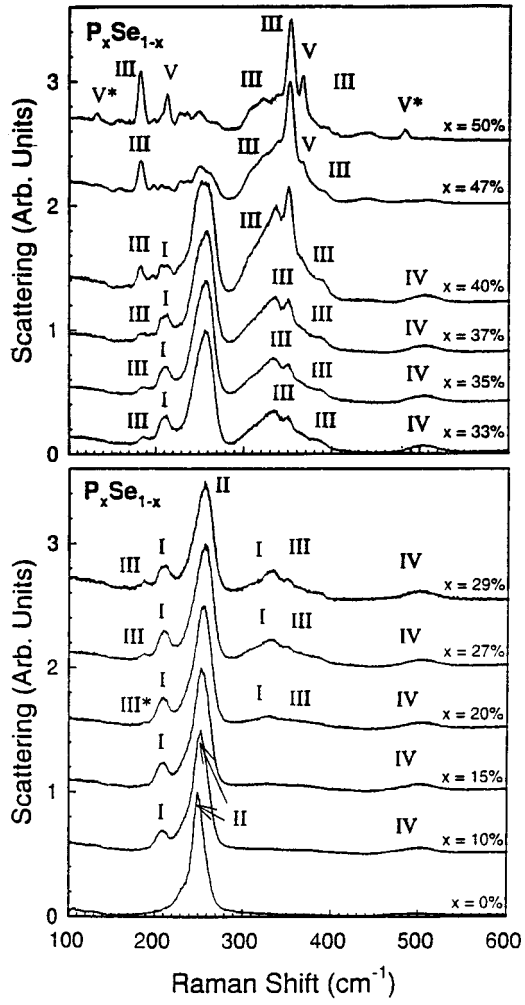

FIG. 3. Raman scattering in P_xSe_{1-x} glasses at the indicated P concentrations. The Raman numerals identify modes of various building blocks which are summarized in Table I. Line shapes at various x are displaced by 0.5 units to assist in viewing.

tical to the ones recorded in quartz ampoules and further revealed no aging effects. All spectra reported here were taken at laboratory ambient.

Figures 3(a) and 3(b) reproduce observed Raman line shapes at selective compositions plotted as a function of P content, starting from pure Se ($x=0$), up to $x=0.50$. Starting from the Se-Se stretch modes at 250 cm^{-1} (labeled II), one sees growth of features labeled I, III, and IV, which are, respectively, identified as modes of pyramidal $P(Se_{1/2})_3$ units, ethylenelike $P_2(Se_{1/2})_4$ units, and quasitetrahedral $P(Se_{1/2})_3Se$ units of the backbone. At $x>0.40$ and in particular at $P_{0.50}Se_{0.50}$, the sharp feature labeled V in Fig. 3(b) is identified with appearances of P_4Se_3 monomer units in these P-rich glasses. Figure 4 plots the fractional area ratio $A_n/A(x)$ of various species $n=$I–V as a function of P concentration x. The Raman line shapes were deconvoluted in terms of a superposition of Gaussians to obtain mode intensities (I_n), frequencies (ν_n), and widths (Γ_n). All three variables were kept floating in the least-squares refinement. The areas are obtained by summing contributions of various Gaussians as-

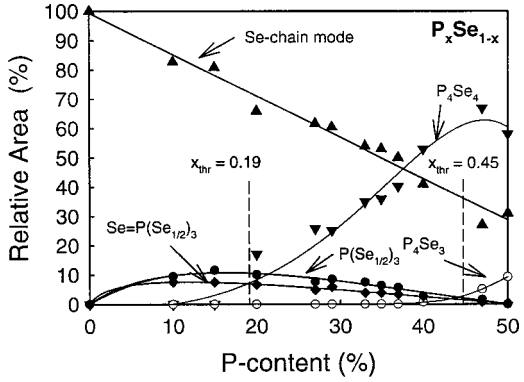

FIG. 4. Relative scattering strengths of various building blocks from Raman spectra of the P-Se glasses.

cribed to a given building block (Table I). We shall return to discuss the justification for the proposed mode assignments (Table I) later.

Figure 5 reproduces Raman line shapes of P-Se glasses in the low-frequency region ($160<\nu<220\,cm^{-1}$) and permits one to track growth of the 188 cm^{-1} mode, which is identified with $P_2(Se_{1/2})_4$ units. These results show that $P_2(Se_{1/2})_4$ units are *first nucleated* in the glasses near $x\simeq 0.20$.

Figures 6(a) and 6(b) reproduce selective regions of the Raman line shapes of P-Se glasses at high P content where modes of P_4Se_3 monomeric units manifest at 132 and 482 cm^{-1}. A perusal of these line shapes shows that the monomer is *first nucleated* near $x\simeq 0.47$ in the glasses. Figure 7 shows spectra of c-P_4Se_3, c-P_4Se_4, and g-P_4Se_4. The spectrum of c-P_4Se_4 is in good agreement with earlier published reports. The spectrum of g-P_4Se_4 is dominated by the modes observed in c-P_4Se_3 and c-P_4Se_4. Raman peaks in the P_4Se_4 glass are in general broader in width than those observed in c-P_4Se_4. In addition, weaker features in the spectrum (in particular, the peak at 250 cm^{-1}) also reveal the presence of structural units richer in Se than the average glass composition.

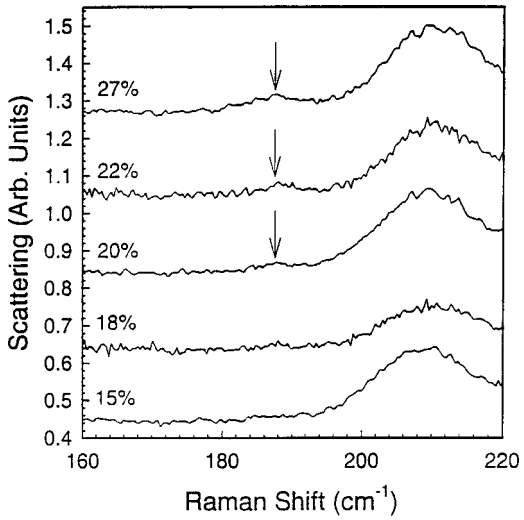

FIG. 5. Nucleation of $P_2(Se_{1/2})_4$ polymeric units in P_xSe_{1-x} glasses at $x>0.20$ as shown by increase in the scattering strength of the 188 cm^{-1} mode (arrow) in Raman scattering.

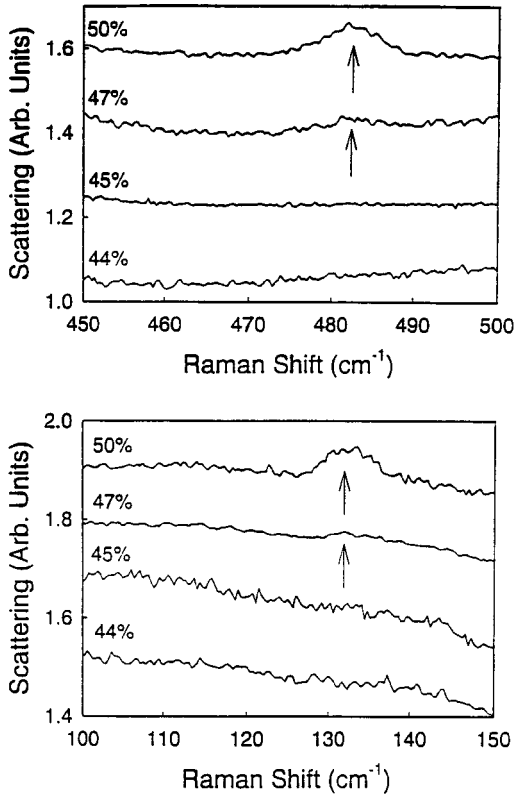

FIG. 6. Nucleation of P_4Se_3 monomers in P_xSe_{1-x} glasses at $x > 0.47$ as shown by an increase in the scattering strength of the 132 cm^{-1} and 482 cm^{-1} modes (arrow) in Raman scattering.

D. ^{31}P NMR spectroscopy and resonance assignments

^{31}P magic-angle spinning (MAS) NMR studies were carried out at 121.5 MHz on a Bruker CXP 300 spectrometer, equipped with a multinuclear 4-mm probe. Spectra were recorded on powdered samples, using 90° pulses of 4 μs length and relaxation delays of 10 min. Typical spinning frequencies were 15.1 kHz. Figure 8 shows representative ^{31}P MAS NMR spectra of P_xSe_{1-x} glasses in the $0.1 < x < 0.4$ concentration range. The results are in good agreement with previous work.[13] At low x, spectra consist of two resonances near zero and 140 ppm, respectively, indicating the presence of two distinct P sites. The high-frequency resonance is assigned to pyramidal $P(Se_{1/2})_3$.[13] This assignment is consistent with the ^{31}P NMR chemical shifts measured on various crystalline model compounds bearing the $P(Se_{1/2})_3$ group.[18] Furthermore, complementary spin-echo decay experiments reveal that in Se-rich glasses, $x < 0.20$, no direct P-P bonds are detected to an appreciable extent.[18,19] The resonance near zero ppm is assigned to tetrahedral $Se{=}P(Se_{1/2})_3$ units. This assignment is more difficult to justify because to date no crystalline model compounds are known, in which P is surrounded by three bridging and one terminal doubly bonded Se atom. Tetrahedrally coordinated PSe_4^{3-} groups do exist, however, in various ternary orthoselenophosphate compounds, and their ^{31}P chemical shifts are generally found within the chemical shift range zero to -100 ppm.[18] Further support for the above assignment comes from the x dependence of the relative peak areas evident from Fig. 8: the experimental species concentrations of the $Se{=}P(Se_{1/2})_3$ units are in quantitative agreement with the corresponding values predicted from an equilibrium model (see below).

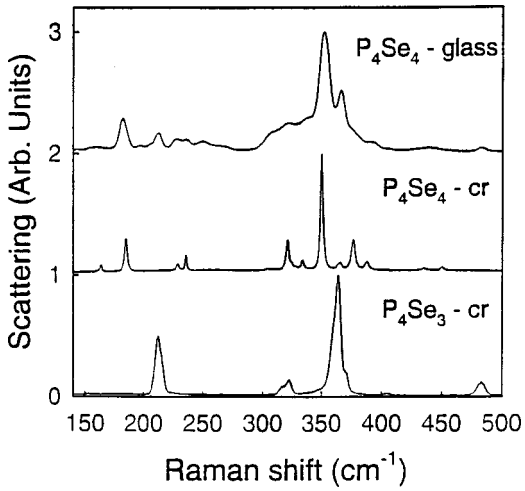

FIG. 7. Comparison of Raman spectra of c-P_4Se_3 and c-P_4Se_4 with g-P_4Se_4. The principal modes observed in the glass can be traced to those in indicated crystals.

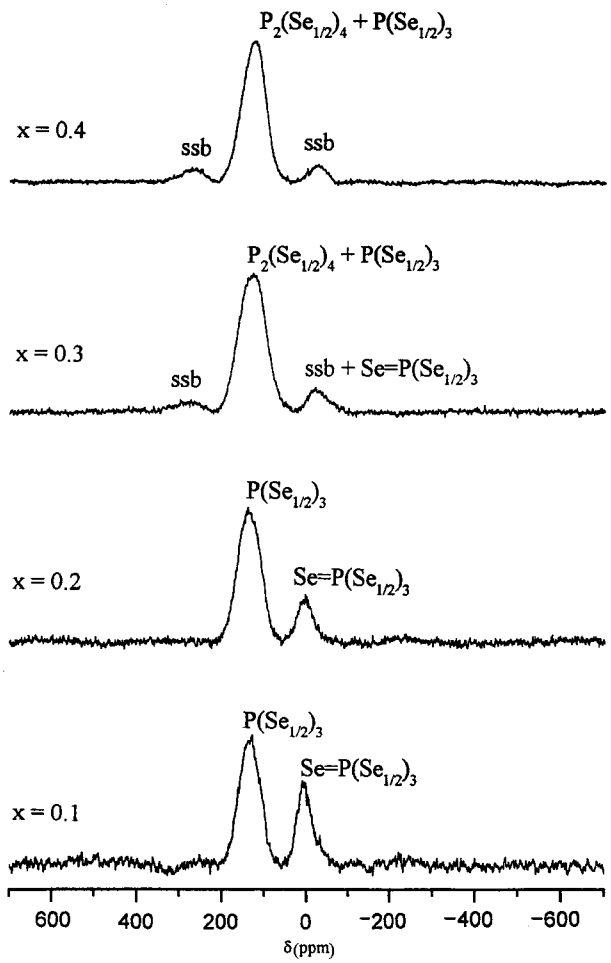

FIG. 8. 121.5 MHz ^{31}P MAS NMR spectra of P-Se glasses as a function of x. "ssb" designates spinning side bands.

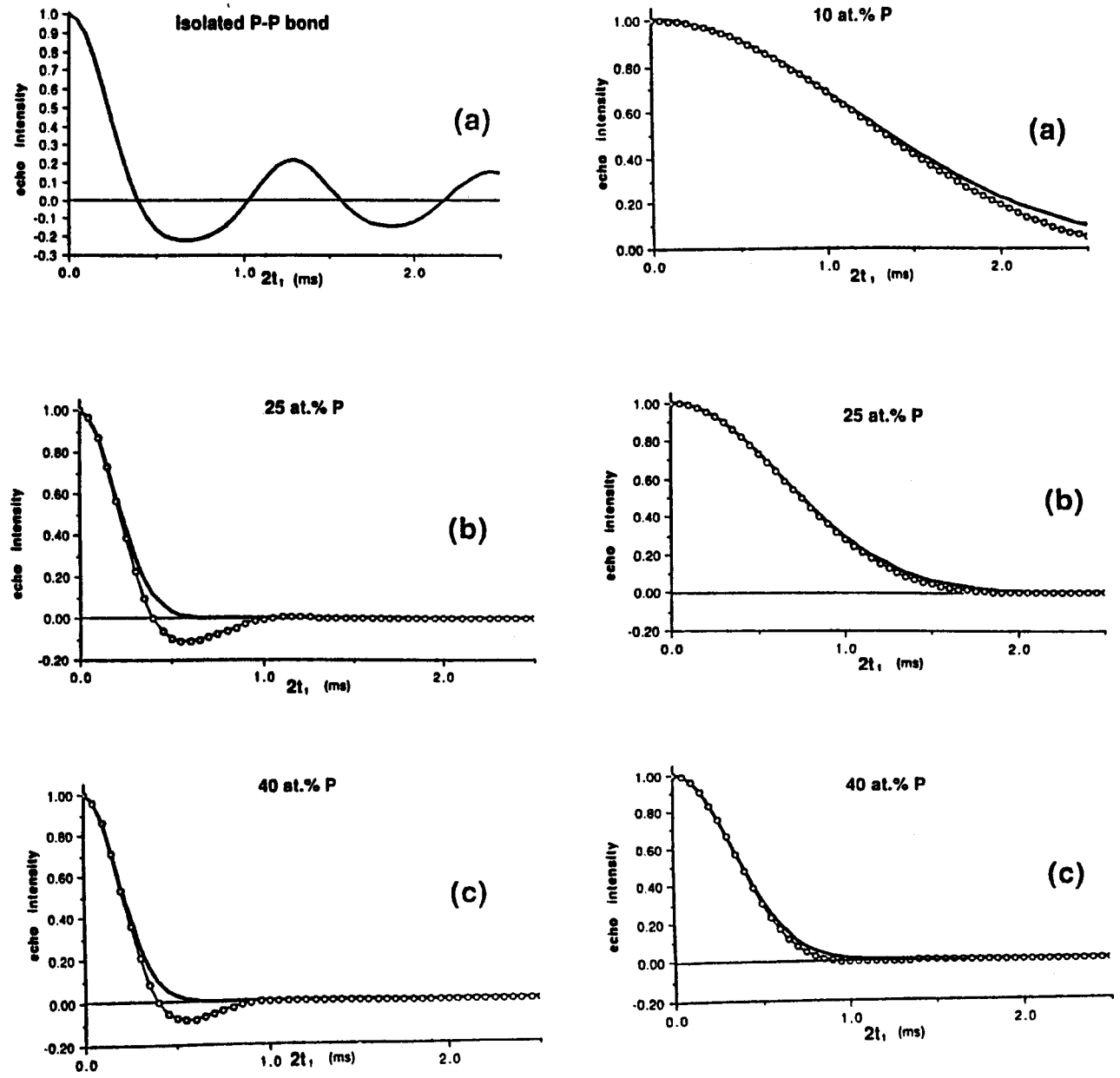

FIG. 9. Predicted ^{31}P spin-echo decay intensity as a function of dipolar evolution time for P_xSe_{1-x} glasses at $x=0.10$, 0.25, and 0.40, respectively. Circles show the result of a rigorous calculation with a single dominant two-spin dipolar interaction, while solid lines represent the approximation of the decay as a Gaussian function. Left side: spin-echo decay for the ethylenelike $P_2(Se_{1/2})_4$ units. Right side: spin-echo decay for $P(Se_{1/2})_3$ units. For additional details see Ref. 18.

Closer inspection of Fig. 8 shows that the center of gravity of the high-frequency resonance is slightly shifted when $x>0.20$. These changes in line shape suggest the appearance of new structural units at higher phosphorus concentrations.

Insights have emerged from ^{31}P spin-echo experiments as previously discussed in detail, the homonuclear ^{31}P-^{31}P dipole-dipole coupling strength can be quantified selectively using a 90°-t_1-180°-t_1 Hahn spin-echo sequence by measuring the spin-echo intensity as a function of the evolution time $2t_1$.[18–20] Since this dipolar interaction is rigorously dependent on the internuclear distance distribution, the experiment differentiates between P-bonded and non-P-bonded types of phosphorus species. This prediction has been verified previously by detailed simulation.[18] The simulations assume that the multispin interaction can be analyzed as a sum of pairwise interactions, resulting in a superposition of oscillatory time dependences of spin-echo decay intensity, where the frequency components depend on the internuclear distances involved and on the orientation of the internuclear vector relative to the magnetic field direction. Following powder averaging, the simulations produce decays of normalized spin-echo intensity as a function of the evolution time $2t_1$, which are summarized in Fig. 9. Here circles show the simulated curves calculated with the assumption of a dominant ^{31}P-^{31}P two-spin interaction, whereas the solid curves are Gaussian approximations to these spin-echo decay curves.

All of the computational details and further assumptions made in these simulations are given in Ref. 18. Figure 9 reveals that the spin-echo intensities for the $P_2(Se_{1/2})_4$ groups (having a strong dipolar interaction owing to the single P-P bond) decay much faster than those predicted for P atoms not involved in direct phosphorus-phosphorus bonding. From a deconvolution of the experimental spin-echo decays into these two distinct contributions, it is then possible to estimate fraction of P atoms involved in P-P bonding. This analysis[18] reveals that P-P bonding starts making a significant contribution to the glass structure at P concentrations above 25 at. %. The quantitative assessment has shown, however, that the extent of P-P bonding is lower than that expected on the basis of merely statistical atomic linking. Assuming, therefore, that homopolar bonding is for the most part limited to one P-P bond per P, we identify this species with a $P_2(Se_{1/2})_4$ group. The results are in excellent accord with Raman scattering observation of a threshold at $x > 0.20$ for the nucleation of this bonding fragment in the glasses. The network structure derives from the crystal structure of polymeric P_4Se_4, which has recently been solved by Ruck.[5] The ^{31}P chemical shifts of *c*- and *g*-P_4Se_4 closely match each other, further supporting the important structural role played by the $P_2(Se_{1/2})_4$ units in this concentration region.

^{31}P MAS NMR spectra at $x > 0.47$ reveal two additional distinct resonances near 65 and -75 ppm in an approximate area ratio of 1:3 (see Fig. 10). These resonances are unambiguously assigned to the apical and basal P atoms of P_4Se_3 monomers, a result in harmony with the Raman observation of a threshold composition $x > 0.47$ for the appearance of the monomer in the glasses. Figure 10 illustrates that the concentration of these units can be influenced by the thermal history of the glass. Here the ^{31}P MAS NMR spectra of a glass at $x = 0.50$ prepared by melting *c*-P_4Se_4 for the duration of 12 h at 350 °C (equilibrated melt) and independently a second sample for 90 min at 340 °C (nonequilibrated melt) are compared: peak integration reveals that upon equilibrating melts by an extended heating contribution of monomeric P_4Se_3 units in the glass increases from 18% to 34%. Both the Raman linewidths and NMR widths associated with P_4Se_3 species are quite narrow and suggest that the underlying molecular unit is decoupled from the glass backbone; i.e., it is monomeric in nature. The intrinsic value of these results on a nonequilibrated melt is that they serve as an important check on our Raman mode and P NMR site assignments in the glasses.

III. DISCUSSION

Some of the issues we will discuss in this section include Raman mode assignments, evolution of glass molecular structure, agglomeration theory and $T_g(x)$ variation, and its consequences on network connectivity.

A. Raman mode assignments

In Table I we have summarized the proposed assignment of modes. In the following we provide some justification for these assignments and, in select cases, the eigenvectors.

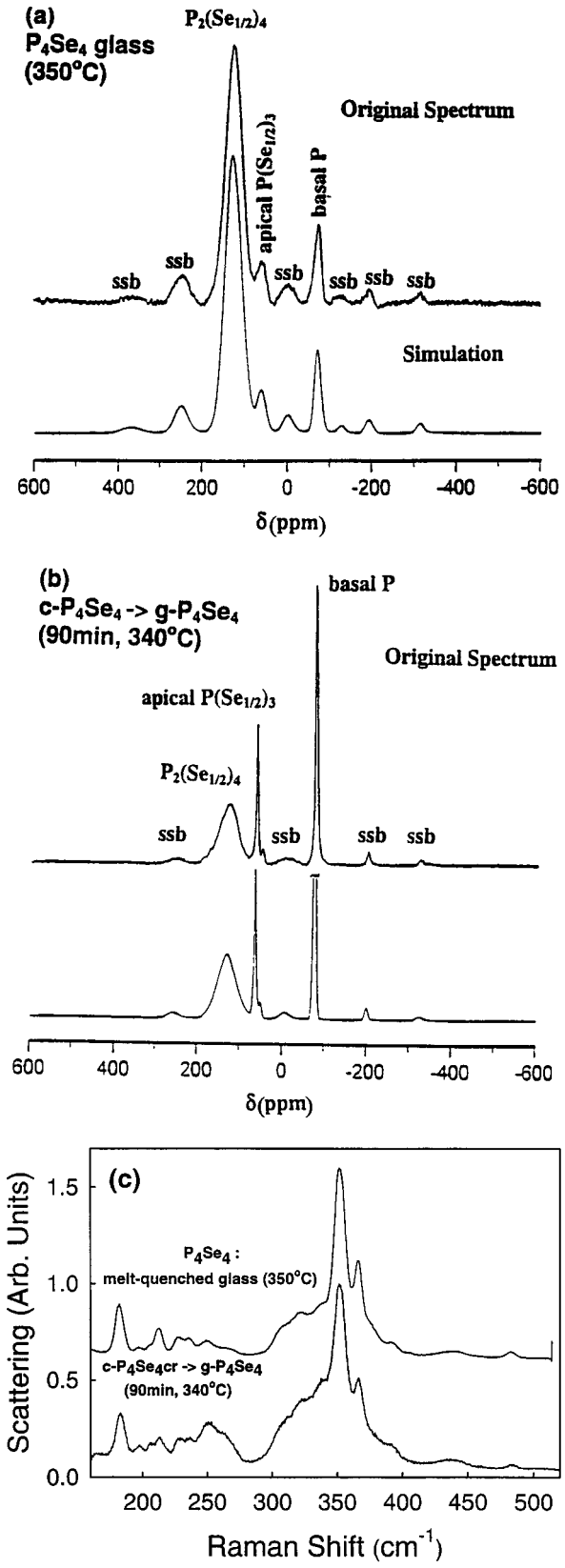

FIG. 10. Effect of thermal history on the ^{31}P MAS NMR spectra (a) and (b) and Raman spectra (c) of $P_{0.5}Se_{0.5}$ glass. (a) NMR glass prepared by melting crystalline P_4Se_4 at 350 °C for 12 h. (b) NMR of glass prepared by melting crystalline P_4Se_4 at 340 °C for 90 min. (c) Raman spectra of corresponding samples.

TABLE I. Raman mode assignments.

	Mode frequency (cm^{-1})	Local unit
I	210, 330	$P(Se_{1/2})_3$ pyramidal units
II	237, 250	Se chains and rings
III	180, 330, 350, 370	$P_2(Se_{1/2})_4$ ethylene like units
IV	510	$Se{=}P(Se_{1/2})_3$ quasi tetrahedral units
V	Narrow modes at 184, 212, 320, 371, 1483	Modes of P_4Se_3 monomer

1. Group I modes: $P(Se_{1/2})_3$ pyramidal units

The pair of modes at 210 and 330 cm^{-1} in the Raman spectra of the glasses are identified with a pyramidal $P(Se_{1/2})_3$ unit and are labeled I in Table I. The eigenvectors of the 330-cm^{-1} mode represent a symmetric breathing of the three Se atoms with the P-cation stationary. The 210-cm^{-1} mode represents an asymmetric stretch of the unit in which the displacement of the P cation is nearly opposite to that of the three Se neighboring anions. These modes are also observed in Raman spectra of c-P_4Se_3 monomer[21] and have been labeled as ν_3 and ν_4, respectively, in Ref. 10.

2. Group II modes: Se_n chain units

The strongly Raman-active band observed near 250 cm^{-1} in the present glasses is traced to a Se-Se stretch in Se_n chains fragments of Se glass.[22] The band is asymmetric and has a lower-frequency companion at 237 cm^{-1} in a Se glass, a feature that apparently persists upon P alloying. We identify band II in Table I as signature of Se_n-chain fragments in the binary glasses.

3. Group III modes: $P_2(Se_{1/2})_4$ polymeric units

The set of modes at 180, 330, 350, 370 cm^{-1} and some weaker ones in between 310 and 340 cm^{-1} are collectively labeled as III in Table I and are identified with the presence of a polymeric network made up of ethylenelike $P_2(Se_{1/2})_4$ units. Support for such identification comes from the Raman scattering results of c-P_4Se_4 and g-P_4Se_4 shown in Fig. 7. The glass obtained by melting the crystal has essentially all the principal modes[17] seen in the crystal, except that they are broadened.

4. Group IV modes: $Se{=}P(Se_{1/2})_3$ units

Although it may be tempting to assign the weak scattering at 510 cm^{-1} to second-order scattering from Se_n chains, the observed trends in scattering strength at 510 cm^{-1} suggest otherwise. The latter shows a maximum at about $x=0.20$ and is thus uncorrelated to the monotonic decrease in concentration of Se_n chains in the glasses with increasing x. The mode at 510 cm^{-1} is identified with a quasi tetrahedral $P(Se_{1/2})_3Se$ unit. A mode at 537 cm^{-1} is observed[23] in some samples of P_4Se_4 and has been identified with the presence of P=Se stretch. The molecular configuration in question[23] is considered to isomerize to the β-P_4Se_4 form.

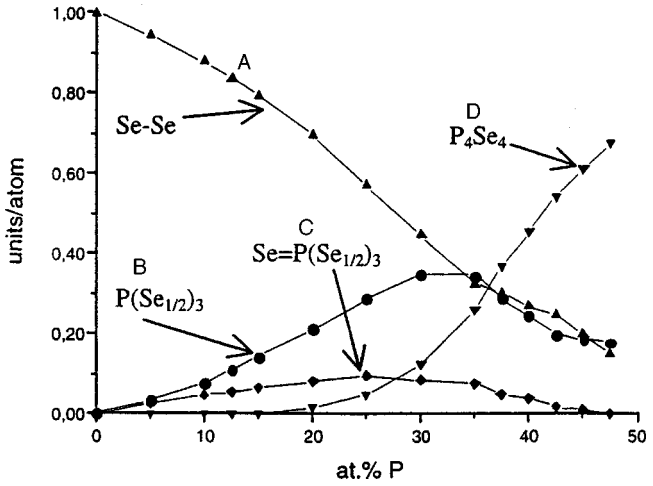

FIG. 11. Indicated species concentrations in P-Se glasses as deduced from NMR spectroscopy: *A*: Se-Se bonds, *B*: $P(Se_{1/2})_3$ units, *C*: $Se{=}P(Se_{1/2})_3$ units. *D*: $P_2(Se_{1/2})_4$ units. For additional details, see Ref. 18.

5. Group V modes: P_4Se_3 monomer units

The sharp peaks appearing at 184, 212, 370, and 483 cm^{-1} labeled collectively as V in Raman spectra of a glass at $x=0.50$ identify the P_4Se_3 monomer. These modes have been previously assigned to ν_9, ν_4, ν_2, and ν_1 vibrations from a normal mode analysis of the monomer in Ref. 21. There is a weakly excited mode at 320 cm^{-1}, labeled as ν_3, which overlaps with a mode of the $P_2(Se_{1/2})_4$ units (group III).

B. Glass structure evolution with P content

Both Raman scattering (Fig. 4) and the ^{31}P NMR (Fig. 11) results independently provide the type and concentration of building blocks in the present glasses. The correlation between the details of glass structure between the two spectroscopies is rather comforting (Figs. 4 and 11). In Raman scattering, the richness of observed line shapes provides a means to directly resolve contributions of various building blocks of the network and, in particular, establish *specific concentrations* where a given building block is first nucleated in the glasses. A disadvantage of the method is that since the observed mode cross sections are never identical, the observed scattering strengths (Fig. 4) can currently only serve as a qualitative measure of concentrations of various species.

Fortunately, the ^{31}P NMR results are, on the other hand, inherently more quantitative. But these experiments do require a combination of measurements to deduce the concentrations of the various units as we discuss below. The spin-echo experiments allow quantification of the $P_2(Se_{1/2})_4$ units, while the MAS NMR spectra serve to quantify the $Se{=}P(Se_{1/2})_3$ groups. All of the P atoms remaining at each glass composition are then attributed to $P(Se_{1/2})_3$ units. Furthermore, by comparing the concentrations with glass compositions, the number of Se-Se bonds can be deduced (Fig. 11). As expected, Se-rich moieties dominate at low P content, whereas the P-bonded species become dominant at $x>0.35$, in harmony with the Raman scattering results (Fig. 4). The

concentration dependence on glass composition is monotonic, and in particular no discontinuity is observed near $x = 0.40$, where a rapid change in T_g is observed (Fig. 2).

The formation of $Se{=}P(Se_{1/2})_3$ groups in the present glasses is of particular interest because, to date, this moiety is *unknown* in the crystal chemistry of phosphorus selenides. In particular, this unit is not present in the molecular structure of P_2Se_5 recently deduced by Blachnik and co-workers.[24] Unlike the situation in the stoichiometrically analogous phosphorus oxide and sulfide, the structure of monomeric P_2Se_5 is based on two $P(Se_{1/2})_3$ units which are connected to each other by bridging selenium atoms and by two diselenide bridges.

Results of Figs. 4 and 11 show that the concentration of $Se{=}P(Se_{1/2})_3$ reaches its maximum value near $x = 0.2$. The concentration dependence of the $Se{=}P(Se_{1/2})_3$ species on x can be modeled quantitatively by assuming the presence of an equilibrium

$$P(Se_{1/2})_3 + Se \leftrightarrow Se{=}P(Se_{1/2})_3, \tag{1}$$

characterized by an equilibrium constant K_I in the vicinity of 0.8.[13,18] This equilibrium is operative in the molten state and is arrested permanently at T_g. Studies in melts ($T > T_g$) have further shown that this equilibrium shifts significantly towards the left as the temperature is increased.[25]

At higher P-content, the glass structure is dominated by the three-fold-coordinated $P(Se_{1/2})_3$ and $P_2(Se_{1/2})_4$ species. Figure 11 also shows that a maximum in the concentration of $P(Se_{1/2})_3$ units is reached near $x = 0.35$; at higher P content, the $P_2(Se_{1/2})_4$ species dominate. Again, these two three-coordinated species can be viewed as being connected by an equilibrium process of the form

$$P_2(Se_{1/2})_4 + Se \leftrightarrow 2P(Se_{1/2})_3. \tag{2}$$

In the case of this equilibrium, however, high-T NMR studies[27] do not reveal any significant T dependence.

P_4Se_3 monomers make a significant contribution to the glass structure only at $x > 0.47$ as also revealed by the Raman results of Figs. 6(a) and 6(b). As Fig. 10 illustrates, the concentration of these units is strongly dependent on the thermal history. Related observations have been made in recent high-T liquid-state ^{31}P NMR studies of P-Se melt containing 48 at. % phosphorus.[25] Furthermore, these liquid-state NMR experiments have also revealed that, although no molecular P_4Se_3 is detected in the glassy state at $x < 0.47$, these species are formed at high temperatures in P-Se melts with x values as low as 0.40. Systematic T-dependent studies reveal the presence of a melt depolymerization equilibrium of the kind

$$3P_2(Se_{1/2})_4 \leftrightarrow P_4Se_3 + 2P(Se_{1/2})_3, \tag{3}$$

resulting in significant changes of the structural specification present. As the temperature increases, the right side of the equilibrium is increasingly favored. From the temperature dependence of the equilibrium constant, a reaction enthalpy value near 50 kJ/mol was obtained.[25]

TABLE II. Parameters y and z for possible and hypothetical molecular units in the P-Se system. Hypothetical molecular units whose identity has not been experimentally documented are marked by asterisks.

Compound	y	z
P_4Se_3	0	0.75
P_4Se_4(M-V)*	0.25	0.75
α-P_4Se_4	0	0.5
β-P_4Se_4	0	0.5
P_4Se_5	0.25	0.5
α-$P_4Se_7^*$	0.5	0.25
β-$P_4Se_7^*$	0.25	0
$P_4Se_{10}^*$	1.0	0
P_2Se_5	0	0

C. Comparison of present structure results with neutron diffraction and EXAFS results

It is instructive to compare glass structure results from the present NMR and Raman results with previous results based on a combined interpretation of neutron diffraction (ND) and extended x-ray-absorption fine-structure (EXAFS) experiments.[7,8] In these previous studies, Price and coworkers have described the structure of the present glasses in terms of two parameters y and z, where y denotes the fraction of four-fold-coordinated P atoms and z the ratio of the number of P-P bonds to the number of P atoms present. They have described their findings with reference to the molecular units P_4Se_3, P_4Se_4 (of which they use the particular isomer proposed by Monteil and Vincent[16]) and P_4Se_5, the structure of which was reported by Penney and Sheldrick.[26] Table II summarizes the parameters y and z represented by these structures. We have further included the y and z parameters for α- and β-P_4Se_4 (Fig. 1), for the molecular structure of P_2Se_5 of Blachnik *et al.*, as well as for two hypothetical structures P_4Se_7 ($x = 0.36$) and P_4Se_{10} ($x = 0.29$).

The comparison of these data illustrates that the speciations derived from NMR and Raman spectroscopies are in good agreement with each other, whereas they deviate substantially from those extracted from the previous ND-EXAFS results. At P content $> 30\,at.\,\%$, ND and EXAFS indicate a substantially higher fraction of four-fold-coordinated P atoms than found in NMR or Raman studies. Furthermore, the number of P-P contacts inferred from the ND-EXAFS results also exceeds that deduced from the present Raman and NMR results at all x. Finally, comparison of Tables II and III illustrates that the values of y and z observed as a function of P content are by and large fairly consistent with the values observed for the various known molecular and crystalline structures in the P-Se system. Contrary to Refs. 7 and 8, we do not observe z to increase as a function of P content in the glasses relative to the crystals. The present results do not support a model of P_4Se_n clusters embedded in a selenium-rich matrix as a possible description of the present glasses.[7,8]

D. Agglomeration theory, slope equations, and $T_g(x)$ variation

The agglomeration theory introduced by Kerner and Micoulaut[15] provides a means to predict $T_g(x)$ trends when

TABLE III. Comparison of y and z deduced from NMR, Raman, and ND and EXAFS (Refs. 7 and 8). n.d. stands for not determined.

x	y (NMR)	y (Raman)	y (Refs. 7, and 8)
0.05	0.43	n.d.	n.d.
0.10	0.37	0.45	n.d.
0.15	0.31	0.4	0.5–0.6
0.20	0.26	0.2	n.d.
0.25	0.22	n.d.	0.25
0.30	0.15	0.15	n.d.
0.35	0.11	0.08	n.d.
0.40	0.05	0.05	0.25
0.45	0.01	n.d.	n.d.
0.50	0	0	0.25(0.2)
x	z (NMR)	z (Raman)	z (Refs. 7, and 8)
0.05	0	n.d.	n.d.
0.10	0	0	n.d.
0.15	0	0	0–0.4
0.20	0	0.25	n.d.
0.25	0.05	n.d.	0.5
0.30	0.12	0.31	n.d.
0.35	0.23	0.38	n.d.
0.40	0.42	0.50	0.75
0.45	0.53	n.d.	n.d.
0.50	0.57	0.55	1.10 (0.9)

agglomeration of atoms or molecules to form a glass network proceeds in a *stochastic fashion*. It is instructive to inquire what message is contained in the observed $T_g(x)$ trend of Fig. 2(a) given the local structural units established from the two spectroscopic probes. To address the issue, we outline the agglomeration theory as it relates to present binary glass system.

The central idea of the theory is to relate an increase of viscosity in a glass-forming liquid with creation of bonds between well-defined *local structural configurations* (LSC's) at random. In the present case, we will consider two LSC's consisting of two-fold-coordinated Se atoms (A) and five-fold-coordinated P atoms (B) as shown in Fig. 12.

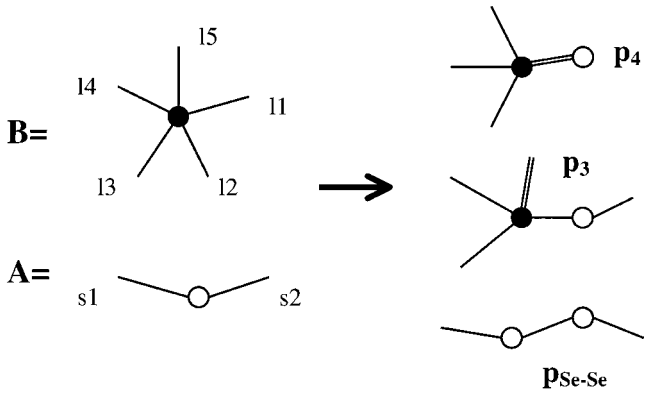

FIG. 12. Linkages of A and B LSC's to produce $Se{=}P(Se_{1/2})_3$ units (P_4) and $P(Se_{1/2})_3$ units (P_3) and Se_n-chain fragments.

Let us consider the statistics of bonding between LSC's in a particular region of a liquid ($T>T_g$) at time $t=0$. Let us denote by $p_A(0)$ (the 0 in the parentheses refers to $t=0$) and $p_B(0)=1-p_A(0)$ the probability distributions for A and B LSC's in the liquid. After a finite step τ_0, these probabilities evolve and acquire new values $p_A(\tau_0)$ and $p_B(\tau_0)$ as bonds reform and LSC's diffuse. Let p_{AA} and p_{AB} designate, respectively, the probabilities for atom A to bond with A and for atom A to bond with B. These probabilities depend on the coordination numbers of atoms A and B, the initial probabilities $p_A(0)$ and $p_B(0)$, and Boltzmann factors which involve bond energies and temperatures. Thus $p_A(\tau_0)$ can be written as

$$p_A(\tau_0)=\frac{1}{2}[p_{AA}+p_{AB}]-p_A(0), \tag{4}$$

At T_g, structural arrest manifests and fluctuations in the probabilities $p_A(\tau_0)-p_A(0)$ must vanish because LSC's cease to move and are trapped. This condition serves to define T_g, as we will see later. In the present binary glass system, at low P content, there are three ways to connect P with Se (we exclude the possibility of P-P bonds): Se-Se, P-Se, and P=Se (Fig. 12). The probabilities $p_{\text{Se-Se}}$, p_3, and p_4 (Fig. 12) of these bonding configurations are given by

$$p_{\text{Se-Se}}(T)=\frac{4}{Z}(1-x)^2 e^{-\beta E_{\text{Se-Se}}}, \tag{5}$$

$$p_3(T)=\frac{12}{Z}x(1-x)e^{-\beta E_{\text{P-Se}}}, \tag{6}$$

$$p_4(T)=\frac{40}{Z}x(1-x)e^{-\beta E_{\text{P=Se}}}, \tag{7}$$

where Z represents the Partition function and $\beta=1/k_BT$.

The Boltzmann factors appearing in Eqs. (5)–(7) take into account bond energies $E_{\text{P-Se}}$, $E_{\text{P=Se}}$, and $E_{\text{Se-Se}}$, while the statistical factors (12, 40, and 4) represent, respectively, the number of equivalent ways to connect a P atom to a Se atom to form single bonds [and create a $P(Se_{1/2})_3$ structural unit] or to form double bonds [and create a $Se{=}P(Se_{1/2})_3$ structural unit], or a Se atom to bond to another Se atom (to form part of a Se chain). These statistical factors can be regarded as *degeneracies* of corresponding energy states of a canonical system (here the different possible bond energies of the network). For simplicity, we will set $E_{\text{P=Se}}=E_{\text{P-Se}}+\Delta$ in the forthcoming. An equivalent way to think is to say that the probability p_{Se} of Se atoms computed from a random distribution of bonds is only equal to the concentration $(1-x)$ of Se, when the entire network becomes connected at T_g. For $T>T_g$, we have $p_{\text{Se}}<1-x$. At $T=T_g$, we have

$$p_{\text{Se}}=\frac{1}{2}[2p_{\text{Se-Se}}+p_3+p_4]=1-x, \tag{8}$$

which gives the same result as $p_A(\tau_0)=p_A(0)$. Equation (8) can be solved exactly from the aforementioned construction and yields

$$x=\frac{3e_{\text{P-Se}}+10e_{\text{P=Se}}-2}{2(3e_{\text{P-Se}}+10e_{\text{P=Se}}-1)}, \tag{9}$$

where $e_{\text{P-Se}}=\exp[-(E_{\text{P-Se}}-E_{\text{Se-Se}})/k_BT_g]$ and $e_{\text{P=Se}}=\exp[-(E_{\text{P=Se}}-E_{\text{Se-Se}})/kT_g]$. One can reduce the number of parameters appearing in Eq. (9) by considering the $x\rightarrow 0$ limit, with the glass transition temperature $T_g\rightarrow T_0$, the glass transition temperature of Se glass. From Eq. (9), we obtain

$$E_{\text{P-Se}}-E_{\text{Se-Se}}=k_BT_0\ln\left[\frac{3+10e^{\Delta/T_0}}{2}\right]. \tag{10}$$

It is convenient to express the energy difference Δ in Eq. (10) in terms of the fraction η of fourfold-coordinated P atoms ($\text{Se}=\text{PSe}_{3/2}$ configurations) in glasses defined as

$$\eta=\frac{p_4}{p_3+p_4}=\frac{10}{10+3e^{\beta\Delta}}. \tag{11}$$

Equation (10) then becomes, in the limit $T_g\rightarrow T_0$

$$E_{\text{P-Se}}-E_{\text{Se-Se}}=k_BT_0\ln\left[\frac{3}{2(1-\eta)}\right]. \tag{12}$$

In Eq. (12), the condition $\eta=1$ is to be excluded, because it implies an infinite value for the energy difference $\Delta=E_{\text{P-Se}}-E_{\text{P-Se}}$, thus leading to a network composed of P=Se links only, which is clearly unphysical. With the energy differences established, Eq. (9) provides a relation between T_g and x with only one parameter, the fraction of fourfold-coordinated P in the glasses.

Finally, the relationship (9) can be cast in a more compact form: if the slope at $x\rightarrow 0$, the origin is computed. Upon the insertion of the established energy difference from Eq. (12), one obtains the final slope equation result:

$$\left[\frac{dT_g}{dx}\right]_{x\rightarrow 0}=\frac{T_0}{\ln\left[\frac{3}{2(1-\eta)}\right]}. \tag{13}$$

At low x, two types of P-cation sites occur and we find that the slope (dT_g/dx) at the origin depends on the parameter η, the fraction of fourfold-coordinated P units. In other chalcogenide systems such as the Ge_xX_{1-x} $(X=\text{S, Se})$, wherein only one cation site is formed, the slope dT_g/dx actually becomes parameter free[28] and equals $T_0/\ln(r_{\text{Ge}}/r_{\text{Se}})=T_0/\ln 2$, in excellent agreement with experiments.

Equation (13) reveals that when $\eta=0$ the slope dT_g/dx equals to $T_0/\ln 1.5$. The slope decreases to $T_0/\ln 3$ at $\eta=1/2$, however. The latter result is not obvious. It is, for example, difficult to see how the connectivity of a network would change by the inclusion of a finite fraction of fourfold-coordinated P atoms ($\eta\neq 0$) in the backbone when these only provide three linkages to the rest of the network, as do the threefold-coordinated P atoms in $\text{P}(\text{Se}_{1/2})_3$ units. The answer resides in the recognition that the presence of fourfold-coordinated P atoms in addition to the threefold-coordinated P atoms drastically *increases the total number of ways* in which P and Se atoms can bond to each other to produce possible clusters. The denominator in the slope, Eq. (13), is related to the entropy of the network. Thus an increase in connectivity of a network can also result from an increase in the number of accessible structural states accounting for a decrease in the slope dT_g/dx at finite x.

^{31}P NMR measurements[11] reveal that η, starting from a value of 1/2 at $x\rightarrow 0$, extrapolates almost linearly to zero as x increases to 0.45. Taking such a variation of $\eta(x)$ into account, we have calculated the expected $T_g(x)$ variation [Eq. (13)] given by the stochastic agglomeration theory. The result is projected in Fig. 2(a) as the dashed line. One finds that the agreement between theory and experiment is excellent at $x\leqslant 0.12$, but at higher x, a systematic deviation sets in. Our interpretation of these results is that in the $0<x<0.12$ composition range, the present glasses can be visualized as a stochastic network composed of Se chain fragments bridging pyramidal $\text{P}(\text{Se}_{1/2})_3$ and quasitetrahedral $\text{Se}=\text{P}(\text{Se}_{1/2})_3$ units in a *random fashion*. At higher x, new building blocks composed of ethylenelike $\text{P}_2(\text{Se}_{1/2})_4$ polymeric units emerge and further reduce the slope dT_g/dx $(0.15<x<0.45)$ by increasing the possible number of pathways in which these three different types of P-centered local units can agglomerate. Stochastic theory suggests that the increase in the number of pathways to agglomerate lowers the slope, dT_g/dx at $x>0.12$. At $x>0.45$, only two building blocks contribute to the network backbone, Se_n-chain fragments and $\text{P}_2(\text{Se}_{1/2})_4$ units, and one finds that the slope dT_g/dx increases drastically as the number of pathways in which clusters can form is severely reduced.

IV. CONCLUDING REMARKS

The rich Raman scattering and ^{31}P NMR line shapes on melt-quenched $\text{P}_x\text{Se}_{1-x}$ glasses have been decoded to yield the concentrations of Se_n-chain, pyramidal $\text{P}(\text{Se}_{1/2})_3$, quasitetrahedral $\text{Se}=\text{P}(\text{Se}_{1/2})_3$, polymeric $\text{P}_2(\text{Se}_{1/2})_4$, and monomeric P_4Se_3 units at $x<0.50$. Such information has provided a means to decode the global connectivity of the backbone and to quantitatively account for the observed T_g variation with x at low x using stochastic agglomeration theory.

ACKNOWLEDGMENTS

It is a pleasure to acknowledge discussions with W. J. Bresser during the course of this work. The work at the University of Muenster was supported by the Deutsche Forschungsgemeinschaft, Grant No. EC168-1, the work at University of Cincinnati by National Science Foundation Grant No. DMR-97-01289, and the work at the Laboratoire de Physique Théorique des Liquides by Center Nationale de Récherche Scientifique Grant No. UMR 7600.

[1] Z. U. Borisova, *Glassy Semiconductors* (Plenum, New York, 1981), p. 70.
[2] G. R. Burns, J. R. Rollo, and R. J. H. Clark, Inorg. Chem. **25**, 1149 (1986).
[3] J. R. Rollo and G. R. Burns, J. Non-Cryst. Solids **127**, 242 (1991).
[4] G. R. Burns, J. R. Rollo, J. D. Sarfati and K. R. Morgan, Spectrochim. Acta, Part A **47**, 811 (1991).
[5] M. Ruck, Z. Anorg. Allg. Chem. **620**, 1832 (1994).
[6] R. Blachnik, P. Lonnecke, and J. Nuss, Z. Anorg. Allg. Chem. **620**, 160 (1994); R. Blachnik and A. Hoppe, J. Non-Cryst. Solids **34**, 191 (1979).
[7] D. L. Price, M. Misawa, S. Susman, T. I. Morrison, G. K. Shenoy, and M. Grimsditch, J. Non-Cryst. Solids **66**, 443 (1984).
[8] M. Arai, R. W. Johnson, D. L. Price, S. Susman, M. Gay, and J. E. Enderby, J. Non-Cryst. Solids **83**, 80 (1986).
[9] D. J. Verrall and S. R. Elliott, Phys. Rev. Lett. **61**, 974 (1988).
[10] R. T. Phillips, D. Wolverson, M. S. Burdis, and Y. Fang, Phys. Rev. Lett. **63**, 2574 (1989).
[11] H. Eckert, Angew. Chem. Int. Ed. Engl. **28**, 1723 (1989).
[12] R. Maxwell and H. Eckert, J. Am. Chem. Soc. **116**, 683 (1994); **115**, 4747 (1993) and references therein.
[13] D. Lathrop and H. Eckert, J. Phys. Chem. **93**, 7895 (1989).
[14] B. Wunderlich, Y. Jin, and A. Boller, Thermochim. Acta **238**, 277 (1994).
[15] R. Kerner and M. Micoulaut, J. Non-Cryst. Solids **210,** 298 (1997); M. Micoulaut Eur. Phys. J. B **1**, 577 (1998).
[16] Y. Monteil and H. Vincent, J. Inorg. Nucl. Chem. **37**, 2053 (1975); also see F. Heyder and D. Linke, Z. Chem. **12**, 480 (1973). Also see Z. U. Borisova, B. E. Kasatkin, and E. I. Kim, Inorg. Mater. (Transl. of Neorg. Mater.) **9**, 735 (1973).
[17] J. D. Sarfati, G. R. Burns, and K. R. Morgan, J. Non-Cryst. Solids **188**, 93 (1995).
[18] D. Lathrop and H. Eckert, Phys. Rev. B **43**, 7279 (1991).
[19] D. Lathrop and H. Eckert, J. Am. Chem. Soc. , 3536 (1989).
[20] D. Lathrop, D. Franke, R. Maxwell, T. Tepe, R. Flesher, Zh. Zhang, and H. Eckert, Solid State Nucl. Magn. Reson. **1**, 73 (1992).
[21] W. Bues, M. Somer, and W. Brockner, Z. Naturforsch. B **35**, 1063 (1980). Also see G. R. Burns, J. Phys. Chem. Solids **47**, 681 (1986).
[22] A. Mooradian and G. B. Wright, in *The Physics of Selenium and Tellurium*, edited by W. C. Cooper (Pergamon, Oxford, 1969), p. 269.
[23] G. R. Burns, J. R. Rollo, J. D. Sarfati, and K. R. Morgan, Spectrochim. Acta, Part A **47**, 811 (1991).
[24] R. Blachnik, H. P. Baldus, P. Lönnecke, and B. W. Tattershall, Angew. Chem. Int. Ed. Engl. **30**, 605 (1991).
[25] R. S. Maxwell and H. Eckert, J. Am. Chem. Soc. **116**, 682 (1994).
[26] G. T. Penney and G. M. Sheldrick, J. Chem. Soc. A **1971**, 245 .
[27] D. Kivelson, S. A. Kivelson, X. Zhao, Z. Nussinov, and G. Tarjus, Physica A **219**, 27 (1995).
[28] M. Micoulaut and G. G. Naumis, Europhys. Lett. **47**, 568 (1999).